Journal of Magnetism and Magnetic Materials 490 (2019) 165547

Contents lists available at ScienceDirect

Journal of Magnetism and Magnetic Materials

journal homepage: www.elsevier.com/locate/jmmm

Research articles

Susceptibility inversion of near-field magnetic sources and its application

Huang Xinjing, Jin Chunxing, Li Jian*

State Key Laboratory of Precision Measuring Technology and Instruments, Tianjin University, Tianjin, China

ARTICLE INFO

Keywords:
Magnetic inversion
Magnetic anomaly
Underground pipeline detections

ABSTRACT

Susceptibility inversion of near-field magnetic sources is of great application significance in the field of magnetic target detections, such as mine clearances and buried pipeline detections. This paper proposes a method of three-dimensional inversion imaging of magnetic sources in near-field with unknown shape, position and magnetization state. The method transforms the total field norm anomaly ΔT on the observation surface into the total field vector anomaly $||\mathbf{T}_a||$ and then constructs an objective function aiming at minimizing the deviations between the measured and predicted magnetic anomalies. The magnetic dipole equivalence principle is utilized to calculate the kernel matrix. The Gauss-Newton and conjugate gradient algorithms are utilized together to solve the inversion optimization process. The range of the magnetic susceptibility is constrained by using nonlinear transformations. Simulations and measurement experiments demonstrate the proposed method is capable to realize 3D inversions of curved pipes, intersecting pipes, separated magnetic sources, and "L" shaped steel pipes under near-field conditions.

Through the actual magnetic field measurement experiments and the implementation of the proposed optimization inversion algorithm, accurate inversion of the magnetic susceptibility distribution and magnetic imaging of the "L" shaped steel tube was realized, testifying that the proposed method is feasible to be applied to the detection of buried pipelines.

1. Introduction

Magnetic detection is a commonly employed way of geophysical explorations, in which magnetic susceptibility imaging is a potential field issue and belongs to quantitative magnetic detection methods [1–4]. This method divides the unknown media space into many meshed elements with discrete magnetic susceptibility distributions, establishes the objective function of susceptibility distributions, and uses the inversion optimization algorithms to solve the susceptibility distributions in the space domain [5–6]. In the traditional inversion method, the magnetization direction of the magnetic source is assumed to be the same as the ambient geomagnetic field. However, in the actual situation, the magnetic source itself may contain original remanent magnetism or interact with other magnetic sources, which can cause original magnetization with unknown directions and reduce the accuracy of magnetic inversions [7]. In order to solve this problem, researchers all over the world have made numerous efforts that can be classified into three kinds of methods.

The first method estimates the magnetization directions of the magnetic source, and then takes the estimated directions as priori information for the 3D magnetic inversion [8]. This method is only suitable for isolated field source in ideal conditions. The second method directly seeks the magnetization vector to obtain both the magnitude and direction of the magnetization intensity at the same time [9]. However, it is usually necessary for this method to add certain constraints to reduce the non-uniqueness caused by the increase in the number of inversion parameters [10]. The third method is the best and most widely used one, which converts the measured magnetic data into the transposition variable that is almost not affected by the magnetization direction. This method requires the least priori information and is suitable for the inversion of multiple and complicated magnetic sources.

For example, Pilkington and Beiki [11] employ inversion algorithms to normalize the magnetic source intensity to reduce the influence of remanence. The total magnetic field norm anomaly ΔT is converted into the magnetic field vector anomaly $||\mathbf{T}_a||$ to implement the magnetic susceptibility inversions. It can suppress the influence of residual magnetism and can be used to obtain the position (or distribution) and the magnetization state of the magnetic body whose magnetization direction is unknown [7,12]. These traditional magnetic inversion methods are mainly used for far-field magnetic source imaging over several kilometers, such as oil and mineral explorations [10,13], the study of magnetic abnormality of the crust and the satellite [14],

* Corresponding author.
E-mail addresses: huangxinjing@tju.edu.cn (H. Xinjing), tjupipe@tju.edu.cn (L. Jian).

https://doi.org/10.1016/j.jmmm.2019.165547
Received 16 January 2019; Received in revised form 11 June 2019; Accepted 7 July 2019
Available online 08 July 2019
0304-8853/

submarine structure surveys and obstacle and shipwreck detection [15,16]. However, they cannot be applied to the inversion imaging of near-field magnetic sources.

The inversion of near-field magnetic source can be used to detect the existence and distribution of possible magnetic sources inside one object without any destruction, which is of great application significance in mine clearances and the exploration of urban underground pipelines. In order to implement the inversion of near-field magnetic sources with unknown magnetization directions, this paper constructs the objective function of the permeability distributions by using the magnetic vector anomaly $\mathbf{T_a}$, determines the kernel matrix of the objective function based on the magnetic dipole equivalence principle, solves optimization inversion equations by using the gauss-Newton and conjugate gradient iteration methods, and testifies the proposed method via both simulations and experiments. The effectiveness of this method is verified in the near-field within two meters, and the 3D inversion of the magnetic anomaly is applied to the near-field magnetic sources with different shapes and layouts. Examples are provided to show how to get the position, distributions, and magnetization state of the underground pipelines by using the magnetic data measured on the ground surface and the proposed inversion method.

2. Method

2.1. Magnetic anomaly characterization

There are two definitions for magnetic anomaly characterization: total field norm anomaly $\Delta T = |||T|| - ||T_0|||$ and total field vector anomaly $T_a = T - T_0$, where T is the total magnetic field and T_0 is the geomagnetic field. In general, $||\mathbf{T}_a||$ is much smaller than the normal field $||\mathbf{T}_0||$, and the direction of $\mathbf{T}_0$ changes very little over a large area, so ΔT can be regarded as a projection of $\mathbf{T}_a$ on $\mathbf{T}_0$, as shown in Fig. 1. Suppose the local geomagnetic inclination is I_0, and the magnetic declination is A_0, then ΔT and $\mathbf{T}_a = (T_{ax}, T_{ay}, T_{az})$ have the following relationship:

$$\Delta T = T_{ax}\cos I_0 \cos A_0 + T_{ay}\cos I_0 \sin A_0 + T_{az}\sin I_0 \tag{1}$$

If the magnetic susceptibility is directly inverted by using ΔT, the result will be very inaccurate due to the influence of the magnetization direction of the magnetic source. It can be proved that the total field vector anomaly $\mathbf{T}_a$ is hardly affected by the magnetization direction of the object [11–12]. When the magnetization direction of the target magnetic source is unknown, inversion of the magnetic susceptibility by using the magnetic anomaly can accurately reveal the shape, position, and magnetization state of the magnetic source.

When the magnetic anomaly $T_a = T - T_0$ is directly measured, the measurement is required to be performed in the same coordinate system, i.e., the three components of the magnetometer probe must be strictly parallel to the East-North-Up world coordinate system. Therefore, it is very likely to cause large errors due to inaccurate movement operations. However, it is relatively easier to accurately measure ΔT. This article will use the relationship between the magnetic field and the magnetic potential, and the spectral differential theorem to convert the measured ΔT to $\mathbf{T}_a$, and then we use $||\mathbf{T}_a||$ to perform the three-dimensional inversion of the

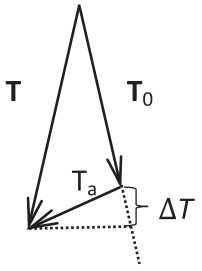

Fig. 1. Relationship of ΔT, $\mathbf{T}_a$, T, $\mathbf{T}_0$.

susceptibility distributions of the magnetic sources [7,17]. The spatial Fourier transform of ΔT is defined as below:

$$S_{\Delta T}(u, v) = \int_{-\infty}^{\infty}\int_{-\infty}^{\infty} \Delta T(x, y) e^{-i_0(ux+vy)} dxdy \tag{2}$$

where i_0 is the unit imaginary number. According to the relationship between the magnetic field and the magnetic potential, the relationship between ΔT and each component of $\mathbf{T_a}$ can be expressed as:

$$\begin{aligned} \frac{\partial \Delta T}{\partial x} &= \frac{\partial T_{ax}}{\partial \mathrm{I}} \\ \frac{\partial \Delta T}{\partial y} &= \frac{\partial T_{ay}}{\partial \mathrm{I}} \\ \frac{\partial \Delta T}{\partial z} &= \frac{\partial T_{az}}{\partial \mathrm{I}} \end{aligned} \tag{3}$$

where $\mathbf{I} = (L, P, Q) = (\cos I_0 \cos A_0, \cos I_0 \sin A_0, \sin I_0)$ is the unit vector in the direction of the geomagnetic field. According to the spectral differentiation theorem, the expression in frequency domain for each component of T_a is [17]:

$$\begin{aligned} S_{T_{ax}}(u, v) &= \frac{2\pi i_0 u}{q_{to}} S_{\Delta T}(u, v) \\ S_{T_{ay}}(u, v) &= \frac{2\pi i_0 v}{q_{to}} S_{\Delta T}(u, v) \\ S_{T_{az}}(u, v) &= \frac{2\pi i_0 (u^2+v^2)^{1/2}}{q_{to}} S_{\Delta T}(u, v) \end{aligned} \tag{4}$$

where $q_{to} = 2\pi[i_0(Lu + Pv) + Q(u^2 + v^2)^{1/2}]$, and u, v are the angular frequencies of x, y, respectively. The three components T_{ax}, T_{ay}, T_{az} of the magnetic anomaly can be obtained via inverse Fourier transform as described by Eq. (5), and then the magnetic anomalous modulus can be obtained as $||\mathbf{T}_a|| = \sqrt{T_{ax}^2 + T_{ay}^2 + T_{az}^2}$.

$$T_{ai}(x, y) = \frac{1}{4\pi^2}\int_{-\infty}^{\infty}\int_{-\infty}^{\infty} S_{T_{ai}}(\omega, v) e^{i_0(\omega x + vy)} d\omega dv \tag{5}$$

where $i = x, y, z$.

2.2. Forward modeling of magnetic anomalies

Assuming that the number of observation points is M, the unknown three-dimensional space to be measured is meshed into N identical cuboid elements, and the unknown spatial permeability distributions are expressed as a column vector in the order of z-x-y: $\mathbf{k} = [k_1, k_2, \cdots, k_i, \cdots, k_N]^T$. The magnetic anomalies at the M observation points can be expressed as a linear function of the magnetic susceptibility k, that is:

$$\mathbf{T}_{ax} = \mathbf{G}_x\mathbf{k},\ \mathbf{T}_{ay} = \mathbf{G}_y\mathbf{k},\ \mathbf{T}_{az} = \mathbf{G}_z\mathbf{k} \tag{6}$$

where $\mathbf{G}_x$, $\mathbf{G}_y$, $\mathbf{G}_z$ are the kernel matrices of $\mathbf{T}_{ax}$, $\mathbf{T}_{ay}$, $\mathbf{T}_{az}$, respectively, with $M \times N$ elements.

Many geological magnetic features are usually similar to the uniform magnetized cuboids, so the magnetic source region is often discretized into many rectangular units and the expression of the induced magnetic field is used to calculate the kernel matrix [18]. Any magnetic body can be regarded as a combination of many small magnet elements, and each magnet element is equivalent to a pair of magnetic dipoles with opposite signs, equal magnetic quantities, and extremely close distances. This paper utilizes the expression of the induced magnetic field based on the magnetic dipole model to calculate the kernel matrix, which can make the inversion model not limited to the rectangular solids or the combination of them, so as to get a result closer to the actual model. Each element of the kernel matrix is calculated as follows [19]:

$$\begin{aligned} G_{xij} &= -\frac{L}{\mathrm{r}^3} + \frac{3(Lx_{ij}^2 + Px_{ij}y_{ij} + Qx_{ij}z_{ij})}{\mathrm{r}^5} \\ G_{yij} &= -\frac{P}{\mathrm{r}^3} + \frac{3(Py_{ij}^2 + Lx_{ij}y_{ij} + Qy_{ij}z_{ij})}{\mathrm{r}^5} \\ G_{zij} &= -\frac{Q}{\mathrm{r}^3} + \frac{3(Lz_{ij}^2 + Py_{ij}z_{ij} + Lx_{ij}z_{ij})}{\mathrm{r}^5} \end{aligned} \tag{7}$$

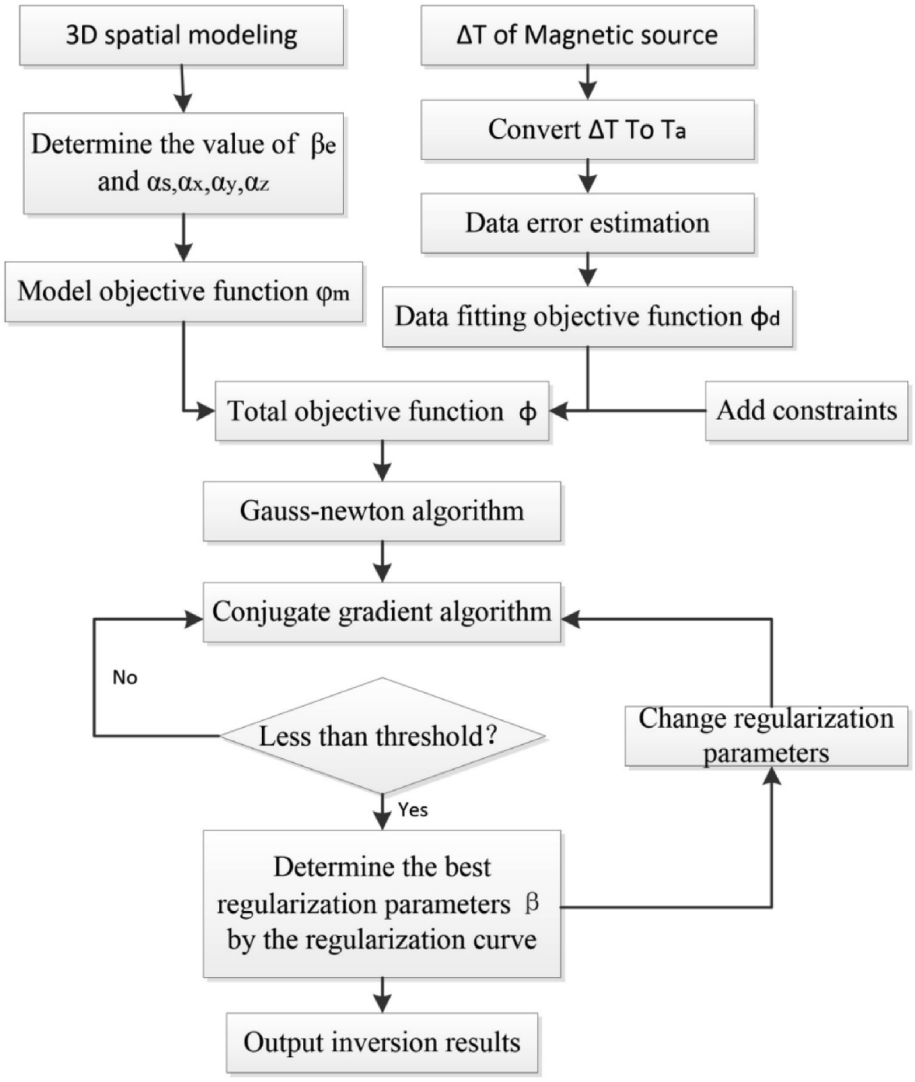

Fig. 2. Flow chart of inversion process.

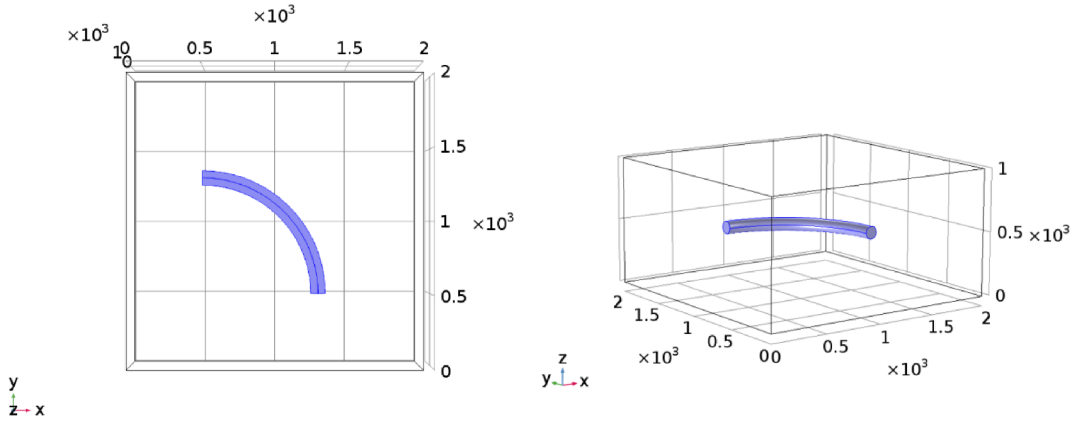

Fig. 3. Quarter-circle simulation model, unit: mm.

where $\mathbf{r}_{ij} = (x_{ij}, y_{ij}, z_{ij})$ represents the position vector of the center point of the *i*th cuboid with respect to the *j*th observation point. The magnetic anomaly modulus $\mathbf{T}_a$ does not have the linear superposition property, and is a nonlinear function of the magnetic susceptibility k. In the inversion process, we need to combine Eqs. (4) and (5) to calculate the kernel matrix of $\mathbf{T}_a$. Let $\mathbf{G}_a$ be the kernal matrix of the magnetic anomaly modulus, that is:

$$\mathbf{T_a} = \mathbf{G_a k} \tag{8}$$

For the kernal matrix $\mathbf{G}_a$ of the magnetic anomaly modulus, its each

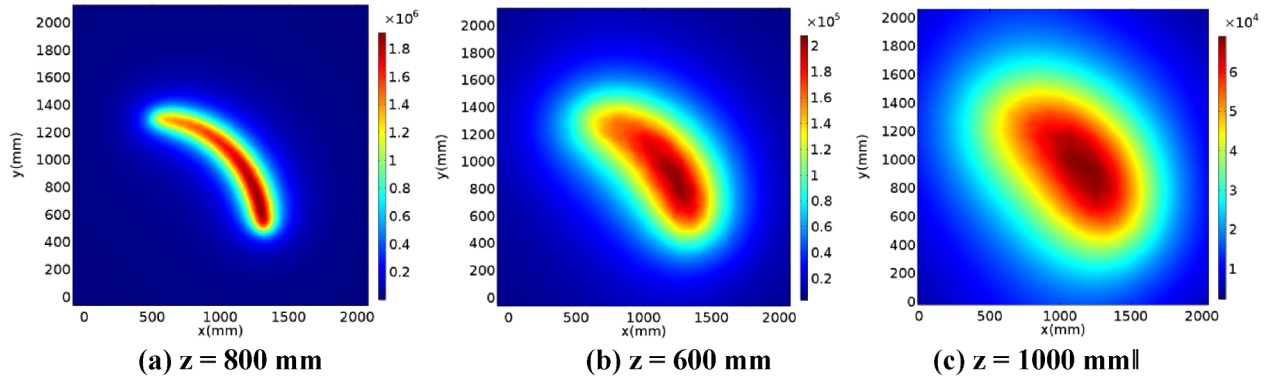

Fig. 4. $||\mathbf{T}_a||$ on the observation plane at different heights (unit: nT).

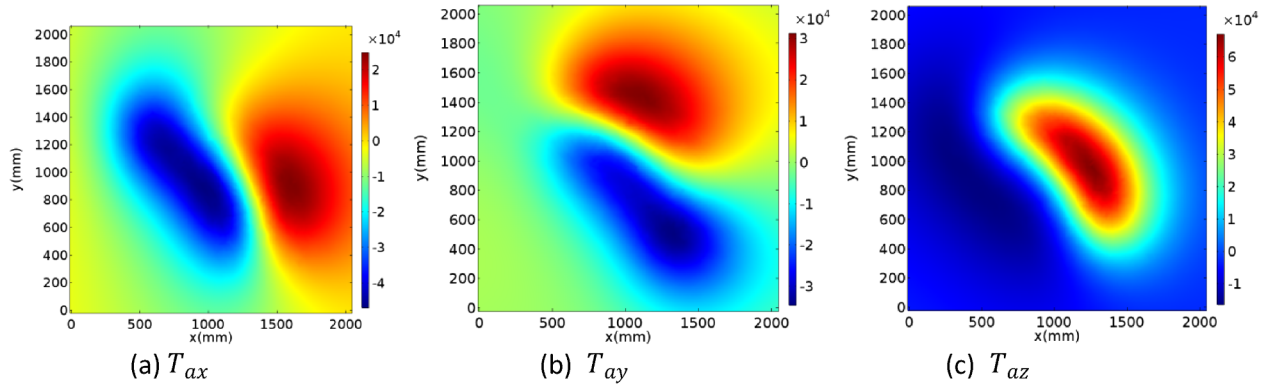

Fig. 5. $\mathbf{T}_a$ on the plane with z = 1000 mm (unit: nT).

element $G_{aij} = \frac{\partial T_{aj}(\mathrm{k})}{\partial k_i}$ represents the change rate of the data at the *j*th observation point with respect to the permeability of the *i*th grid, whose expression is [17]:

$$G_{aij} = \frac{1}{||T_{aj}||}\{T_{axj},\ T_{ayj},\ T_{azj}\}\cdot\{G_{xij},\ G_{yij},\ G_{zij}\} \tag{9}$$

In the optimization calculation process, $||\mathbf{T}_{aj}|| = \sqrt{T_{axj}^2 + T_{ayj}^2 + T_{azj}^2}$ uses the value obtained from the previous iteration. Only calculations of three matrices G_x, G_y, G_z are needed in the inversion process, which can speed up the calculation process. Since $\mathbf{T}_a$ is a nonlinear function with respect to the magnetic susceptibility **k**, the sensitivity matrix $\mathbf{G}_a$ is no longer a constant matrix and will change with the change of the magnetic susceptibility k during the iterative process.

2.3. Optimization process for the permeability inversion

The forward modeling of magnetic anomalies follows the Coulomb law of magnetic fields, and the magnetic anomalies generated by any three-dimensional magnetic source can be obtained by making volume integral of the magnet elements. Minimizing the difference between the magnetic anomalies from measurement and forward prediction is taken as the goal of optimization, and the optimization objective function is established as Eq. (10) [5,6]:

$$\min\varphi(\mathbf{k}) = \varphi_d + \beta\varphi_m = \sum_{j=1}^{M}\left(\frac{\mathbf{T}_{\mathrm{aj}}^{\mathrm{obj}} - \mathbf{T}_{\mathrm{aj}}^{\mathrm{pred}}}{\varepsilon_{\mathrm{j}}}\right)^2 + \beta\left\{\begin{array}{l}\alpha_s\int |\mathrm{w}(z)(\mathbf{k}-\mathbf{k_{ref}})|^2 dv + \\ \alpha_x\int\left|\frac{\mathrm{w}(z)\partial(\mathbf{k}-\mathbf{k_{ref}})}{\partial x}\right|^2 dv + \\ \alpha_y\int\left|\frac{\mathrm{w}(z)\partial(\mathbf{k}-\mathbf{k_{ref}})}{\partial y}\right|^2 dv + \\ \alpha_z\int\left|\frac{\mathrm{w}(z)\partial(\mathbf{k}-\mathbf{k_{ref}})}{\partial z}\right|^2 dv\end{array}\right\} \tag{10}$$

s. t. $\mathbf{k}_{min} < \mathbf{k} < \mathbf{k}_{max}$

Among them, φ_d is the data fitting objective function, which can make the magnetic data produced by the inversion model to accord with the observation data; φ_m is the model objective function, by using which a solution that satisfies the model objective function in infinite solutions can be found, which can decrease the degrees of freedom in inversion; $\beta > 0$ is a regularization parameter to weigh the weights between φ_d and φ_m. When β is too small, the fitting of observation data will be excessive; when β is too large, the weight is biased towards the model objective function, which means the fitting of observation data is insufficient and the model of the inversion structure will be too smooth and simple. This paper uses the Tikhonov regularization curve to determine β, and assume the value of β at the suddenly increasing point of the curve (at the inflection point) as the optimal value [20].

In φ_d, *M* is the number of data from observation; $\mathbf{T}_{\mathrm{aj}}^{\mathrm{obj}}$ is the observed data, which is obtained through transformation of ΔT that is measured; $\mathbf{T}_{aj}^{pred}$ is the predicted data obtained from forward modeling, and is calculated by $\mathbf{T}_{\mathrm{a}}^{\mathrm{pred}} = \mathbf{G_a}\bullet\mathbf{k}$, where is the kernel matrix of $\mathbf{T}_a$, and **k** is the magnetic susceptibility obtained by inversion; ε_{j} is the standard deviation of the error of the *j*th observation data. Because the observed data often contains high frequency noises, if ε_{j} is not used in (10) or its value is too small, overfitting of the observation data will occur; if its value is too large, the inversion result will be deviated from the actual result due to the loss of valid observation data.

In φ_m, the first line is the minimum model objective function in order to ensure that the reconstructed model is the smallest model and the corresponding coefficient is α_s; The 2–4 lines is the smooth model objective function, it calculates the least square value of the model differential in the three directions of *x*, *y* and *z* to ensure the model smoothness and that the values of adjacent model parameters do not abruptly change; and the corresponding coefficients are α_x, α_y, α_z respectively. When α_s/α_x, α_s/α_y, α_s/α_z are larger, the inversion model is closer to the minimum model, so the smoothness will get damaged; when the ratio is low, the inversion model can deviate from the minimum model. This paper lets $\alpha_s = 0.0001$, $\alpha_x = 2$, $\alpha_y = 2$, $\alpha_z = 2$

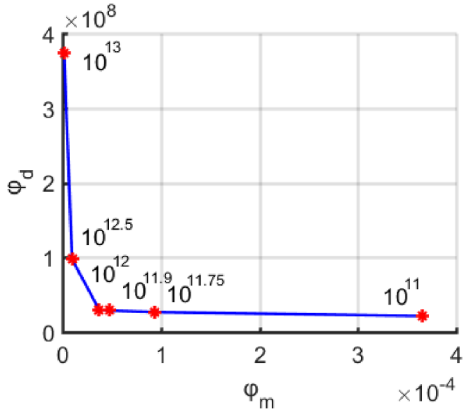

Fig. 6. Regularized curves of the magnetic susceptibility inversion for the quarter ring.

[21–22]. $\mathbf{k}_{\text{ref}}$ is a reference susceptibility model, and this paper takes $\mathbf{k}_{\text{ref}} = 0$. $\omega(z)$ is a depth-weighted function [23]. Since the influence of the magnetic source body on observation data cubically decays as the distance increases, a depth weighting function can be introduced to avoid the skin effect of the inversion result. The expression of $\omega(z)$ is:

$$w(z) = w(z_i + z_0) = \sqrt{\frac{1}{(z_i + z_0)^{\beta_e}}} \tag{11}$$

where z_i is the depth of the ith spatial model element, and z_0 is the height of the observation plane. For the observed height and magnetic anomaly modulus data in this paper, the most accurate inversion result can be obtained when β_e is about 5. The optimization process of the magnetic permeability inversion is as follows (see Fig. 2):

For linearizing the nonlinear equations, we use the Gauss-newton algorithm to solve the objective function $\varphi(\mathbf{k})$ by gradual iteration in the optimization algorithm. The Gauss-Newton iteration algorithm has the advantages of fast convergence and high accuracy. The conjugate gradient iteration algorithm is used to solve the high-dimensional linear equations. The conjugate gradient iteration algorithm has the characteristics of small storage required, step convergence and high stability, and does not require any external parameters. The magnetic susceptibility is constrained by nonlinear transformation [24] to avoid negative value. This method takes advantage of the logarithm, constrains the magnetic susceptibility within the boundary range step by step during the iteration, and can avoid the nonlinear problems caused by the logarithmic barrier method [22].

3. Simulation validations

The finite element simulation software COMSOL was used to calculate the magnetic field distributions around the models of one quater ring, two separated cuboids, and intersecting pipes. The ring, cuboids and pipes are all emerged in air domain. The surface of the air domain is configured as the external magnetic flux density. The air domain size is determined when its size increases the simulation results no longer change. Background magnetic field is applied to the steel and air domains according to the local geomagnetic field. The domains are meshed into triangular elements under an "Extremely fine" size configuration. Via finite element simulation, magnetic source inversion was performed to verify the reliability of the proposed method. Each case was deployed in two steps: (1) simulate the forward modeling process to obtain observation data and add white noises to the data to act as real measured data. (2) Use the observed data to perform three-dimensional inversion of the magnetic sources.

3.1. Quarter ring

The finite element simulation was used to calculate the magnetic field distribution around a quarter of a circle. The height of the ring is 500 mm, the main radius of the ring is 800 mm, and the radius of the section is 50 mm. The magnetic susceptibility of the model is set to 300 SI, the remaining space is the background field domain with a constant magnetic susceptibility of 0 SI. The inversion space is divided into $20 \times 20 \times 10 = 4000$ cubes with a geometric dimension of 100 mm × 100 mm × 100 mm. The X axis is set as pointing to the geographical north, the Y axis is set as pointing to the geographical east, and the Z axis is set as pointing down. The observation planes were taken as $z = 600$, 800, and 1000 mm respectively. Background ground field is set as $I_0 = 45^\circ$, $A_0 = 5^\circ$, $T_0 = 5000$ nT (see Fig. 3).

The calculated magnetic anomaly modulus $\|\mathbf{T}_a\|$ caused by the quarter circle at different observation heights are shown in Fig. 4 below. It can be seen when the observation plane is close enough to the quarter circle, the shape and position of the magnetic source can be clearly determined only by the distribution of $\|\mathbf{T}_a\|$. When the observation plane is far from the model, the shape and position of the magnetic source cannot be directly judged from $\|\mathbf{T}_a\|$ hence magnetic inversion is needed. Therefore, the distance of the observation surface from the magnetic source is set far enough in both the simulation and the experiment for verifying the inversion performances. $\|\mathbf{T}_a\|$ on the plane with z = 1000 mm, which is furthest away from the magnetic source, is selected for inversion. The data of the components T_{ax}, T_{ay}, and T_{az} on the observation surface are shown in Fig. 5 below.

5% of the means of T_{ax}, T_{ay} and T_{az} are added to each component of $\mathbf{T}_a$ as Gaussian random noises of standard deviations. The noise-doped data are used to perform the inversion process. The regularization

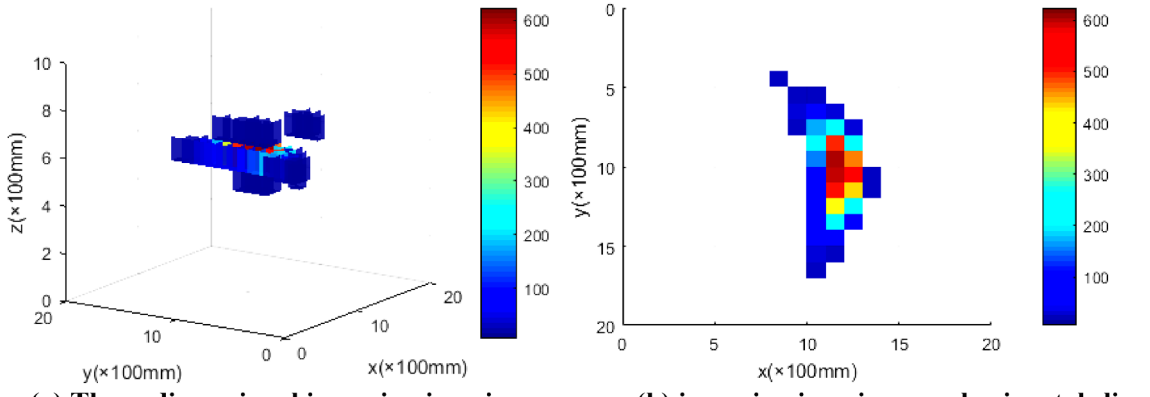

(a) Three-dimensional inversion imaging **(b) inversion imaging on a horizontal slice**

Fig. 7. Calculated susceptibility of a quarter-circle when $k_{\max} = 600$.

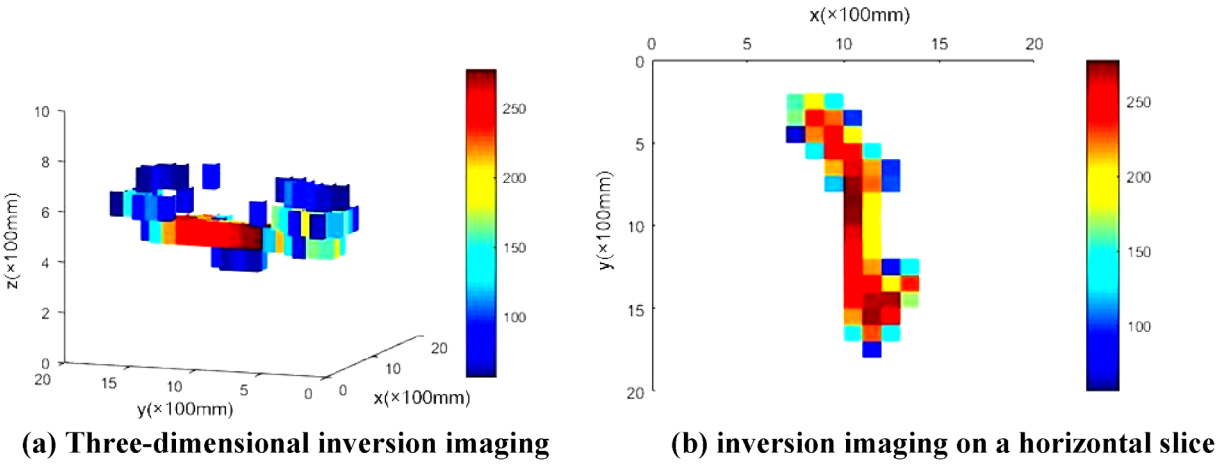

Fig. 8. Calculated susceptibility of a quarter-circle when k_{max} = 300.

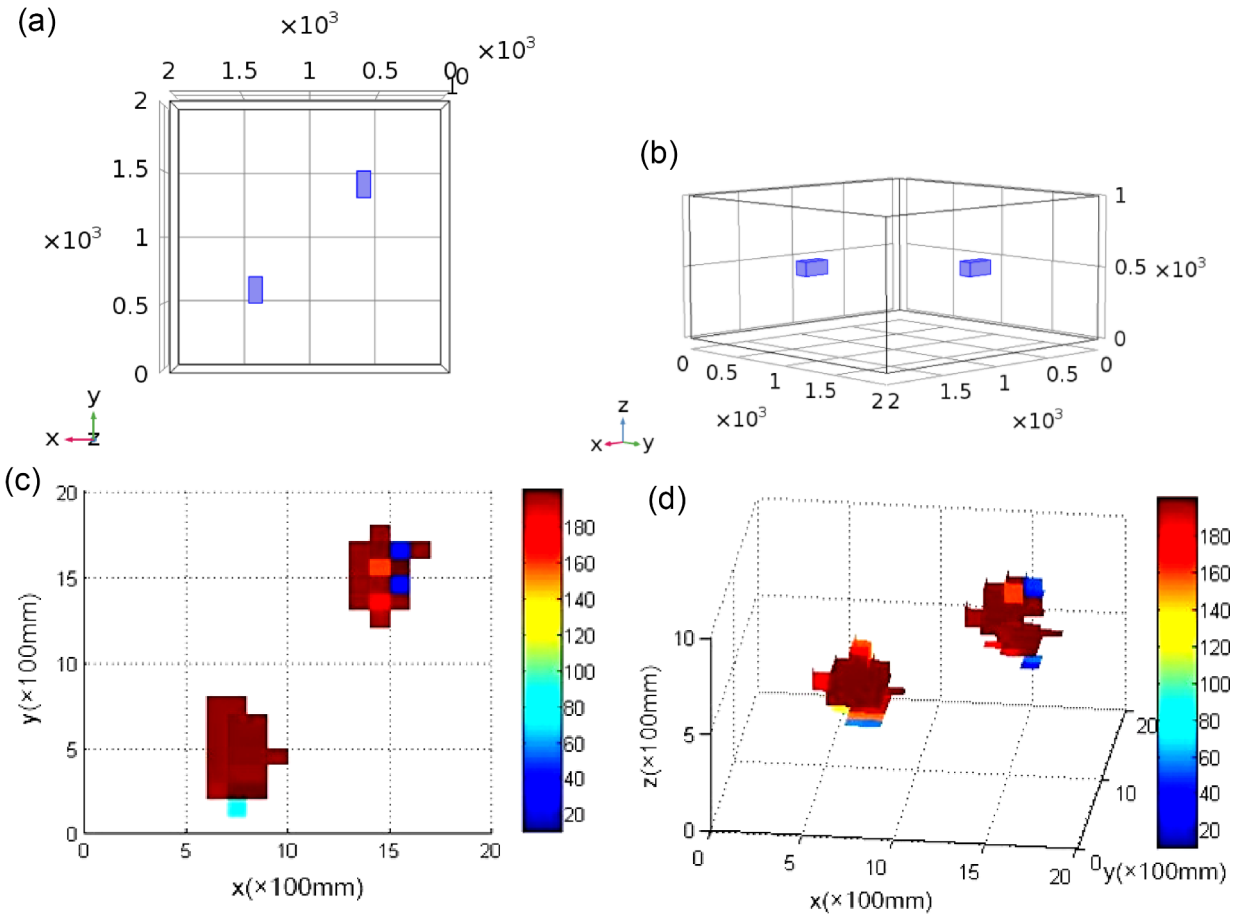

Fig. 9. Magnetic susceptibility inversion results of two cuboid models: (a) XY Plane View of the simulation model (unit: mm); (b) Three-Dimensional View of the simulation model (unit: mm); (c) Horizontal slice of susceptibility inversion results (SI); (d) Three-dimensional inversion imaging (SI).

parameter β is swept from 10^{11} to 10^{15}. The regularization curve of multiple inversions is plotted in Fig. 6. The best regularization parameter of this model is about $\beta = 10^{12}$ at the inflection point of the curve. Remove the points in the inversion results whose susceptibility is equal or less than 0.1% of the maximum value of calculated susceptibility, and the new results are shown in Fig. 7.

As can be seen from Fig. 7, the model shape of the inversion source is close to that of the real model, but the overall susceptibility distribution is very uneven, and it is much less than 600. Therefore, the k_{max} can be intentionally reduced to focus on the inversion model, in order to improve the inversion accuracy of the susceptibility. The above inversion process is repeated again with k_{max} = 300. After removing the points in the inversion results whose susceptibility is equal or less than 0.1% of the maximum value of the maximum calculated susceptibility, the new results are shown in Fig. 8. It can be seen this inversion method can accurately recover the shape and position of a curved bar.

3.2. Two cuboid models

The dimensions of the two rectangular parallelepiped models are

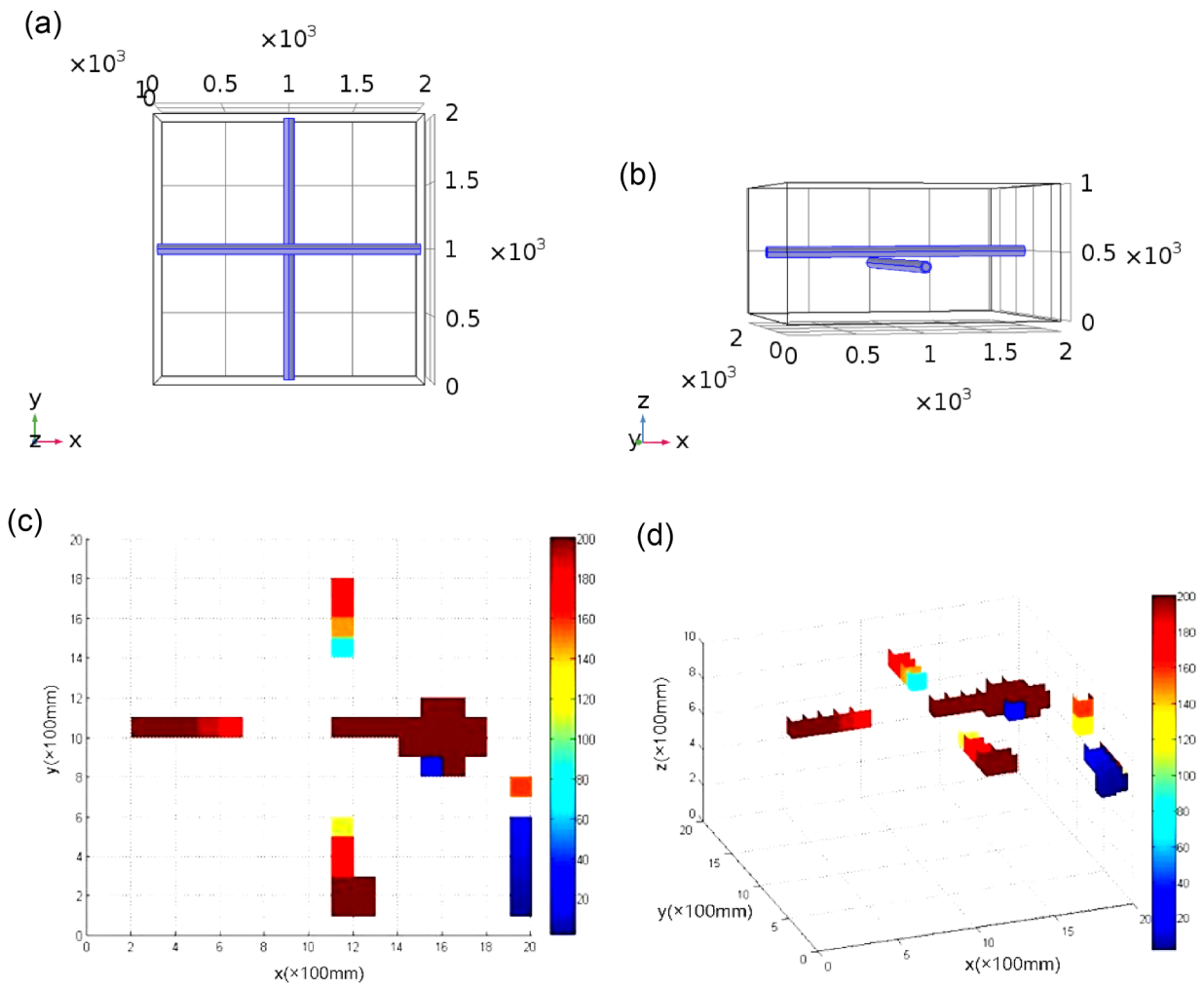

Fig. 10. Magnetic susceptibility inversion results for the cross-pipe model: (a) XY Plane View of the simulation model (unit: mm); (b) Three-Dimensional View of the simulation model (unit: mm); (c) Horizontal slice of susceptibility inversion results (SI), geometric unit: 100 mm; (d) Three-dimensional inversion imaging (SI), geometric unit: 100 mm.

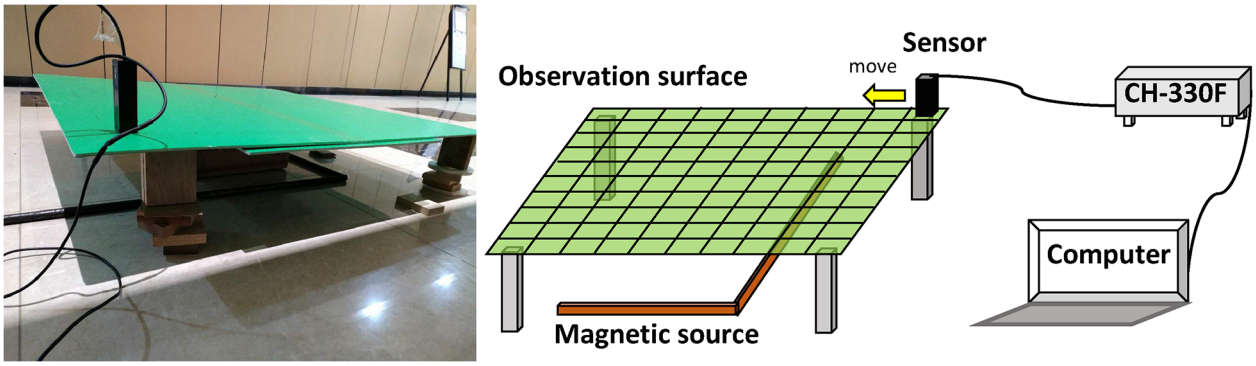

Fig. 11. Experimental apparatus and measurement schematic.

200 mm × 100 mm × 100 mm, as shown in Fig. 9. The cuboid center coordinates are (1400 mm, 600 mm, 500 mm) and (600 mm, 1400 mm, 500 mm), respectively. The magnetic susceptibility of the two blocks is set to 300 SI, and the magnetic susceptibility of the remaining space is set to 0 SI. The observation plane is at $z = 1000$ mm, and the background magnetic field is set to $I_0 = 45^\circ$, $A_0 = 5^\circ$, $T_0 = 5000$ nT. With k_{max} taken as 200, after the same inversion steps, remove the points in the inversion results whose susceptibility is equal or less than 0.1% of the maximum value of the calculated susceptibility, the new results are shown in Fig. 9. It can be seen this algorithm can accurately locate the positions of the two magnetic sources in space. The size of the inversion image is 2–3 times larger than the actual magnetic source size, and the magnetic susceptibility is smaller than the actual value.

3.3. Cross pipe model

The crossover pipe model is shown in Fig. 10. The two pipes are the same size, with the outer radius of 40 mm, the inner radius of 30 mm,

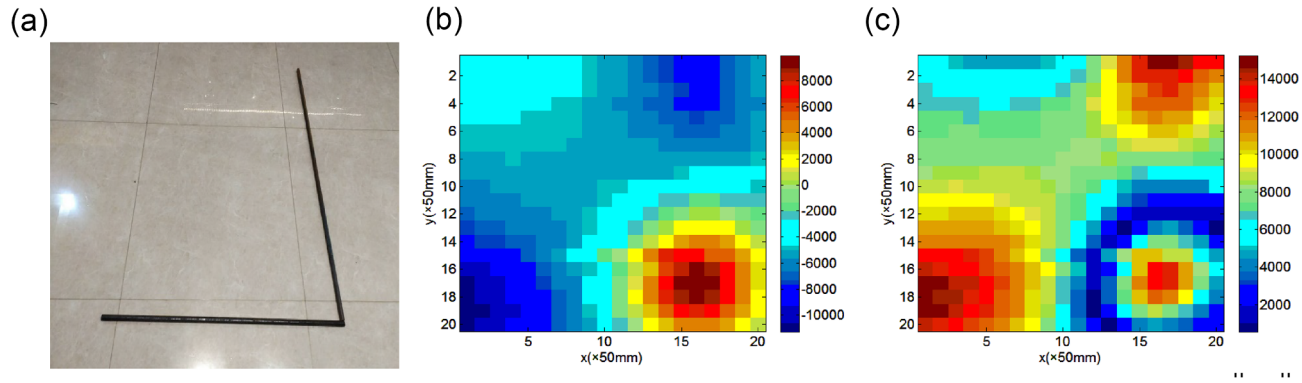

Fig. 12. Magnetic anomaly modulus of "L" shaped pipe (a), and measured $\Delta \mathbf{T}$(b) and transformed $||\mathbf{T}_a||$ (c) on the observation plane, (unit: nT).

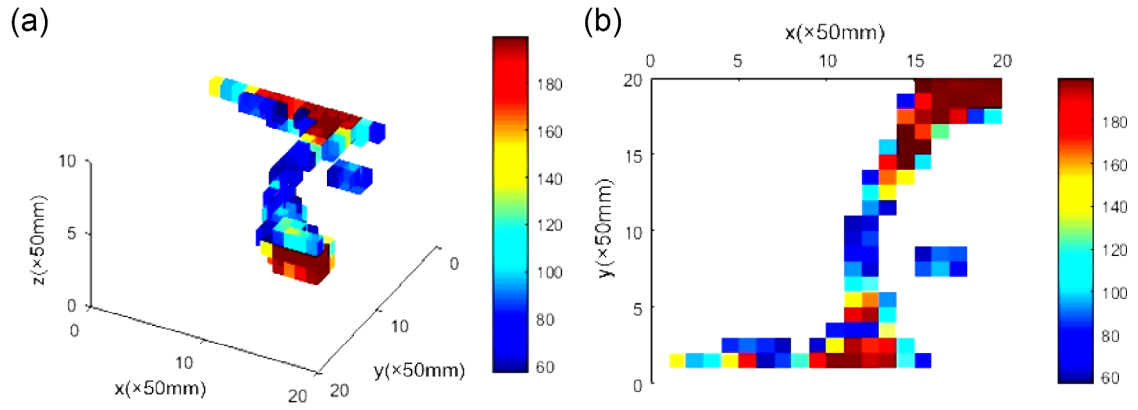

Fig. 13. Magnetic susceptibility inversion results for the "L" shaped pipe: (a) Three-dimensional inversion imaging (unit: SI); (b) Horizontal slice of susceptibility inversion results (unit: SI).

and the length of 2000 mm. The two pipes are perpendicular to each other and their heights are respectively 500 mm and 400 mm. The susceptibility of the model is set to be 300, the remaining space is the background field, and the magnetic susceptibility is set to 0. The observation plane is selected as $z = 600$ mm (see Fig. 11).

The inversion results are shown in Fig. 10(c) and (d). The depths of the two pipes of the actual model are not the same, but the two pipes in the inversion results are in the same plane. The inversion results of the lower pipe lose the middle segment, and the inversion susceptibility is smaller than that of the upper pipe. The inversion results can accurately reflect the positions of the two pipes, and distinguish the depth difference between the two pipes in terms of the magnetic susceptibility distribution. Due to the meshing resolution limitation, the results cannot reveal the hollow features of the magnetic source.

4. Application experiments

In order to verify the practicability of the inversion method, we built a test system. The magnetic susceptibility inversion was used to realize the detection of the position and distribution of the underground pipeline. We select two steel tubes with the outer diameter of 20 mm and the inner diameter of 18 mm, one of which is 900 mm long and the other is 1200 mm long. The two steel tubes were collocated into an "L" shape and the observation surface was set 300 mm far from the steel pipe. The area of 1 m^2 on the observation surface was divided into 400 small square grids, each of which has a size of 50 mm × 50 mm. The magnetometer used in the experiment was CH-330F, a high-precision flux-gate meter with basic accuracy of ± 0.10% of reading and a resolution of 0.01 nT. The magnetic sensor probe was placed in the exact center of each grid while measuring and the probe was always kept in one direction. The measurement data was sent to the laptop in real time and was displayed and stored in real-time by using the Labview program. The mean value of a series of data with a stable display was taken as the value of the total magnetic field modulus at each observation point.

Subtract the magnitude of geomagnetic field 50,000 nT from the 400 magnetic field data measured and we can get the magnetic anomaly modulus at each point on the observation surface which is shown in Fig. 12. Using the method mentioned above to convert the ΔT measured to $||\mathbf{T}_a||$, and the result is shown in Fig. 12(b) and (c).

Substitute the local geomagnetic field direction of the experiment site $I_0 = 57.9°$, $A_0 = 5.8°$ into the inversion process, and remove the data in the inversion results lower than the background value. The background value is set as 5% of the maximum susceptibility obtained by the inversion. The inversion imaging results is shown in Fig. 13.

The results can indicate the approximate shape and susceptibility distribution of the pipeline. It can be seen that the magnetization state of the steel pipe is not very uniform, and the magnetic susceptibility at the corner of the "L" shaped steel pipe is greater than the other parts of the pipe body. Due to the steel pipe that is placed parallel to the Y-axis is longer than 1 m, which exceeds the observation surface boundary, there is a redundant part in the upper right corner of the inversion results, which deteriorates the overall inversion results. However, during the actual process of underground pipeline detections, the length of the pipeline often exceeds the range of the observation surface. The results show that the proposed method can still invert the correct position and susceptibility distribution of the pipes in this case.

In field application, linear array or planar array consisting of many magnetometers is required to enhance measurement efficiency. The signal quality of magnetic field measurement can be guaranteed via measures in three aspects: (1) Calibration in advance to ensure high precision and consistency of the magnetometers; (2) Posture of the

array carrier should be stable enough to ensure that the measuring coordinate system of the magnetometer is invariable; (3) The measuring carrier itself cannot cause a strong magnetic field. A non-magnetic towfish as the measuring carrier can be employed and dragged via a zero-density rope that is linked to the underwater robot or the vessel. The rope is soft and long enough so that the magnetometer postures on the towfish will not be interfered by the movement of the robot and the vessel, and the magnetic anomalies caused by the robot and vessel will not be perceived by the magnetometer either.

5. Conclusions

In this paper, we study the three-dimensional inversion imaging of magnetic source with unknown shape, position and magnetization state under a near-field condition. The method transforms the total field norm anomaly ΔT on the observation surface into the total field vector anomaly $||\mathbf{T}_a||$ and then constructs an objective function aiming at minimizing the deviations between the measured and predicted magnetic anomalies. We utilize the magnetic dipole equivalence principle to calculate the kernel matrix, utilize the Gauss-Newton algorithm and the conjugate gradient algorithm together to solve the inversion optimization process, and constrain the range of the magnetic susceptibility by using nonlinear transformation.

Through simulations and measurement experiments, the proposed method is demonstrated to be capable to realize 3D inversions of curved pipes, intersecting pipes, separated magnetic sources, and “L” shaped steel pipes under near-field conditions. The shape and susceptibility distributions of “L” shaped steel pipes are accurately detected and located through actual magnetic measurement experiments and implementing optimization algorithms. If the mesh is further refined, the inversion accuracy can be improved, but the calculation burden will be greatly increased and the inversion time will be longer.

Acknowledgements

This work is supported by National Natural Science Foundation of China (Nos. 51604192, 61773283) and Project funded by China Postdoctoral Science Foundation (No. 2018M630271).

References

[1] M. Pilkington, 3-D magnetic imaging using conjugate gradients, Geophysics 62 (4) (1997) 1132–1142.
[2] M. Pilkington, 3D magnetic data-space inversion with sparseness constraints, Geophysics 74 (1) (2009) L7–L15.
[3] Gang Yin, Yingtang Zhang, Hongbo Fan, Guoquan Ren, Zhining Li, Automatic detection of multiple UXO-like targets using magnetic anomaly inversion and self-adaptive fuzzy c-means clustering, Explor. Geophys. 48 (1) (2018) 67–75.
[4] Matthias Weigel, Oliver Bieri, Spinal cord imaging using averaged magnetization inversion recovery acquisitions, Magn. Reson. Med. 79 (4) (2018) 1870–1881.
[5] C.L. Yao, T.Y. Hao, Z.N. Guan, Y. Zhang, High-speed computation and efficient storage in 3-D gravity and magnetic inversion based on genetic algorithms, Geophysics 46 (2) (2003) 252–258.
[6] C.L. Yao, Y.M. Zheng, Y.W. Zhang, 3-D gravity and magnetic inversion for physical properties stochastic subspaces, Geophysics 50 (5) (2007) 1576–1583.
[7] Y.G. Li, S.E. Shearer, M.M. Haney, N. Dannemiller, Comprehensive approaches to 3D inversion of magnetic data affected by remanent magnetization, Geophysics 75 (1) (2010) L1–L11.
[8] P.G. Lelièvre, D.W. Oldenburg, A 3D total magnetization inversion applicable when significant, complicated remanence is present, Geophysics 74 (3) (2009) L21–L30.
[9] R.G. Ellis, B. de Wet, I.N. Macleod, Inversion of magnetic data from remanent and induced sources, Aseg Extended Abstr. 2012 (1) (2012) 1–4.
[10] S.L. Li, Y.G. Li, Inversion of magnetic anomaly on rugged observation surface in the presence of strong renmnent magnetization, Geophysics 79 (2) (2014) J11–J19.
[11] M. Pilkington, M. Beiki, Mitigating remanent magnetization effects in magnetic data using the normalized source strength, Geophysics 78 (3) (2013) J25–J32.
[12] S.E. Shearer, Three-dimensional inversion of magnetic data in the presence of remanent magnetization, Master’s thesis Colorado School of Mines, 2005.
[13] M. Muhammad Fawzy Ismullah, Muhammad Altin Massinai Maria, Shallow depth study using gravity & magnetics data in Central Java – Yogyakarta, J. Phys. 97 (9) (2018) 012–046.
[14] J.S. Du, Study on processing, forward modeling and inversion algorithms of satellite magnetic anomaly data in spherical coordinate system, Acta Geod. Cartogr. Sin. 44 (2) (2015) 236.
[15] S.L. Li, Y.G. Li, X.H. Meng, The 3D magnetic structure beneath the continental margin of the northeastern South China Sea, Appl. Geophys. 9 (3) (2012) 237–246.
[16] B.L. Lv, Study on the underwater objects key technologies for detecting using the magnetic survey and their applications, Ph.D. Thesis China University of Geosciences, 2015.
[17] S.B. Liu, 3D magnetic susceptibility imaging based on the amplitude of magnetic anomalies, Ph.D. Thesis China University of Geosciences, 2011.
[18] Y. Luo, C.L. Yao, Theoretical study on cuboid magnetic field and its gradient expression without analytic singular point, Oil Geophys. Prospect. 42 (6) (2007) 714–719.
[19] O. Portniaguine, M.S. Zhdanov, 3D magnetic inversion with data compression and image focusing, Geophysics 67 (5) (2002) 1532–1541.
[20] A. Tikhonov, V. Arsenin, Solutions of Ill-posed Problems, V H Winston and Sons, 1977.
[21] Y.G. Li, D.W. Oldenburg, 3-D inversion of gravity data, Geophysics 63 (1) (1998) 109–119.
[22] Y.G. Li, D.W. Oldenburg, Fast inversion of large-scale magnetic data using wavelet transforms and a logarithmic barrier method, Geophys. J. Int. 152 (2) (2003) 251–265.
[23] Y.G. Li, D.W. Oldenburg, 3-D inversion of magnetic data, Geophysics 61 (2) (1996) 394–408.
[24] V.C.F. Barbosa, J. Silva, W.E. Medeiros, Gravity inversion of a discontinuous relief stabilized by weighted smoothness constraints on depth, Geophysics 64 (5) (1999) 1429–1437.

Huang Xinjing received his B.S. and Ph.D degrees at Tianjin University in 2010 and 2016, respectively. He is now an Assistant Professor and master advisor of the major of instrument science and technology at Tianjin University. His research interests involve analyses of the magnetic field inside and outside the pipeline and its application in the detection and location of pipeline damage.

JinChunxing received her B.E. degree in 2016, from Tianjin University. She is now a master at the School of Precision Instrument and opto-electronics engineering, Tianjin University. Her research interests include underground pipe location and susceptibility detection.

Li Jian received his B.E., M.E., and Ph.D. degrees in 1994, 1997 and 2000 respectively, all from Tianjin University. He is now a Professor and doctoral supervisor, at the School of Precision Instrument and opto-electronics engineering, Tianjin University. His research interests include pipeline leak detection, pipeline safety warning, and novel in-pipe detector. He is the corresponding author of this paper.